Kinematics of the viscous filament during the droplet breakup in air

Diana Broboana
Polytechnic University of Bucharest
Ana-Maria Bratu
Polytechnic University of Bucharest
Istvan Magos
Polytechnic University of Bucharest
Claudiu Patrascu
Polytechnic University of Bucharest
Corneliu Balan (corneliu.balan@upb.ro)
Polytechnic University of Bucharest

Research Article

Keywords: dripping regime, thinning velocity, rheology

Posted Date: October 8th, 2021

DOI: https://doi.org/10.21203/rs.3.rs-955518/v1

Version of Record: A version of this preprint was published at Scientific Reports on February 2nd, 2022.
See the published version at https://doi.org/10.1038/s41598-022-05839-y.

Kinematics of the viscous filament during the droplet breakup in air

Diana Broboana, Ana-Maria Bratu, István Magos, Claudiu Patrascu, Corneliu Balan[1]

The dripping regime in the vicinity of droplet breakup is analyzed concerning the evolution of the filament's neck and its corresponding thinning velocity. Three flow regimes are observed as the relative time decreases: (i) a monotonous increase of the neck's thinning velocity, where inertia and capillarity are balanced, (ii) a transition region characterized by the equilibrium between inertia, capillarity, and viscous forces, where the thinning velocity varies non-monotonically with the relative time and (iii) the final pinch-off regime, where velocity decreases or oscillates around a constant value. Based on the correlation between experimental data and numerics, the distribution of the ζ - coefficient (defined as the non-dimensional second invariant of the velocity gradient) on the droplet's profile is used to quantify the ratio between elongation and rotation of the fluid at the interface. The regions dominated by extension, where pure elongation is located at $\zeta \cong 1$, are determined. One main result of this study is the confirmation that distribution of the ζ - coefficient is a relevant parameter to analyze and to quantify the breakup process. This result has the potential of developing novel techniques and more precise procedures in determining the interfacial rheology of viscous and complex fluids.

The stretching of filaments and breakup of droplets have been intensively studied in the last decades. Past studies have shown that universal exponents emerge when using scaling functions that characterize the pinch-off process[1]. The pinch-off is directly related to droplet formation and its subsequent filament thinning stages[2-5], most of them being correctly described by nonlinear theories[6]. Given that Weber number remain below 4, the injection of a fluid will manifest as a dripping regime. For a low viscosity fluid, transitions from dripping to jetting are characterized by the dependence between Weber and Bond numbers[7]. Other types of transitions have also been identified and associated with droplet formation or with the breakup process of a contracting liquid filament[8-12].

One of the main targets of past studies has been the relation between the dynamics of the filament, from its formation to the pinch-off, with the extensional properties of the fluid sample. The investigations of viscoelastic filaments thinning include: the rheology of transient filament thinning processes[13,14], the dependence of the diameter profile on the molecular weight of the polymer[15,16], the deformation of sheer-thinning liquid bridges[17], the capillary breakup of weakly elastic fluids and CaBER experiments[18-20], regime identification[21], the influence of an external liquid[22-24], and drop dynamics[25,26]. The applicative potential is related to material characterizations and the measure of relaxation time[16,27,28], ink-jet printing technologies[29], extensional rheology of suspensions[30], dysphagia nutritional support[31,32], microfluidic devices[33-36], and use of surfactants[37]. The break-up of liquid filaments formed when a droplet detaches still proves to be a vast field of study. Subject to an asymmetric tension, the filament may or may

[1] University Politehnica of Bucharest, Faculty of Power Engineering, REOROM Laboratory, Splaiul Independentei 313, 060042 Bucharest, Romania. Correspondence and requests for materials should be addressed to C.B. (email: corneliu.balan@upb.ro).

not decay in accordance with theoretical predictions. Here we show similarities and limitations of filament thinning theories derived to tackle symmetric threads.

The paper is concerned with the experimental investigation and the numerical modeling of the breakup process of a viscous filament surrounded by air. The goal of the paper is to determine the kinematics of a liquid filament, previously to the droplet detaches from a capillary needle. After the calibration of the numerical solutions with experiments, there are analyzed the evolution of filament's profile and local velocities distributions on the filament's interface. The proposed kinematics quantity to characterize the filament interface during thinning are: (a) the minimum diameter thinning velocity and (b) the distribution of the ζ – coefficient (a non-dimensional second invariant of the velocity gradient), which indicates where exist possible regions with pure extensional flows.

Methods

The experimental and numerical investigations of the droplet formation and the detachment of the droplet from the capillary in air are performed in a confined geometry. The constant flow rate of the liquid sample is imposed in a capillary needle with the inner diameter $d_0 = 2.21\ mm$ using a Harvard syringe pump, the mean velocity inside the needle being maintained constant $v_0 = 10\ mm/s$, Fig. 1a. To avoid possible external perturbations due the air current, the needle is fixed in the middle of a glass tank with 200 mm height and square cross section of 150 mm × 150 mm. As the liquid leaves the needle it forms a droplet which then detaches under its own weight, leaving behind a liquid filament that progressively thins until rupture. Snapshots of the phenomenon are then obtained using two high-speed cameras: Phantom VEO-E 340L (resolution of 1280×1000 pixels at 2000 fps, pixel size 10 microns) and FASTCAM mini-UX100 (1280 x 1024 pixels at 4000fps, pixel size 10 microns). The scale of each picture is set by the outer diameter of the needle, $d_{ext} = 2.7\ mm$. The minimum neck diameter (d_{min}), the distance between the apex of the drop and the needle (L) and the maximum droplet diameter (D), as shown in Fig. 1a, are then measured using the ImageJ or Matlab softwares, the two fluids in contact being identified with black and white colors, respectively. The pixel dimension corresponding to the ImageJ resolution is 20 μm. The errors in measurements appear due to the presence of the "grey" pixels at the boundary between the two fluids in contact (generated by optical interference/reflection). The image processing performed in the Matlab environment is based on the binarization technique, Fig. 1a-d. To determine the binary threshold, a detail is extracted from the area of the filament interface from the original image, Fig. 1a. The obtained image is negativated (Fig. 2b) and the line of pixels corresponding to the minimum diameter of the filament is represented graphically (Fig. 2c) to observe the transition more easily from background to object. It is considered that the interface starts at the pixel with the first value other than 0 and ends at the pixel whose value is 50 less than that of the next pixel. The two determined values (T_1 and T_2, respectively) represent the ends of the range that includes the pixel values at the interface. The binarization threshold is considered the arithmetic mean of the ends of this interval. The final image (Fig. 2d) is obtained by binarization of the original image with the found threshold. The band between T_1 and T_2 cover 3 pixels, therefore the error in determining the interface is approximately 30 μm.

Non-stationary solutions of the Navier-Stokes equations (Newtonian fluids under incompressible and isothermal conditions) for the whole flow domain are obtained with the commercial Fluent code, the dynamics of the droplet

interface being computed using the VoF model.[38-41]. The time step is 0.1 ms with 400 maximum iterations per time step and 10^{-8} precision. The geometry is axial-symmetric and contains almost 300.000 quadrilateral cells. The working PC has 16 parallel processors at 3 GHz and 128 GB RAM memory. For one case, the necessary computation time to obtain the rupture/detachment of the jet/droplet from the capillary is at least 25 days. The boundary conditions are (i) no slip at the solid wall, (ii) free surface at the upper limit of the domain, (iii) constant velocity at the entrance of the capillary, (iv) a 90° contact angle between the tested fluid and the capillary wall (considered with zero thickness). The interface between the immiscible fluids was traced using the VoF implicit scheme at a volume fraction (VF) of 0.5. The errors in the measurements of the interface profile are given by the width band between VF = 0.1 and VF = 0.9, which for thin filaments covers almost 50% from the nominal measured dimension, Fig. 1e. The limit of our calculus is established by the mesh quality (the number of nodes/cells) and directly related with the computation time step and the available resources.

The tested sample is a viscous Newtonian silicon oil with the following material properties (measured at temperature of 23° C: density – $\rho = 870\ kg/m^3$, viscosity – $\eta = 0.2\ Pas$ and surface tension – $\sigma = 0.025\ N/m$.

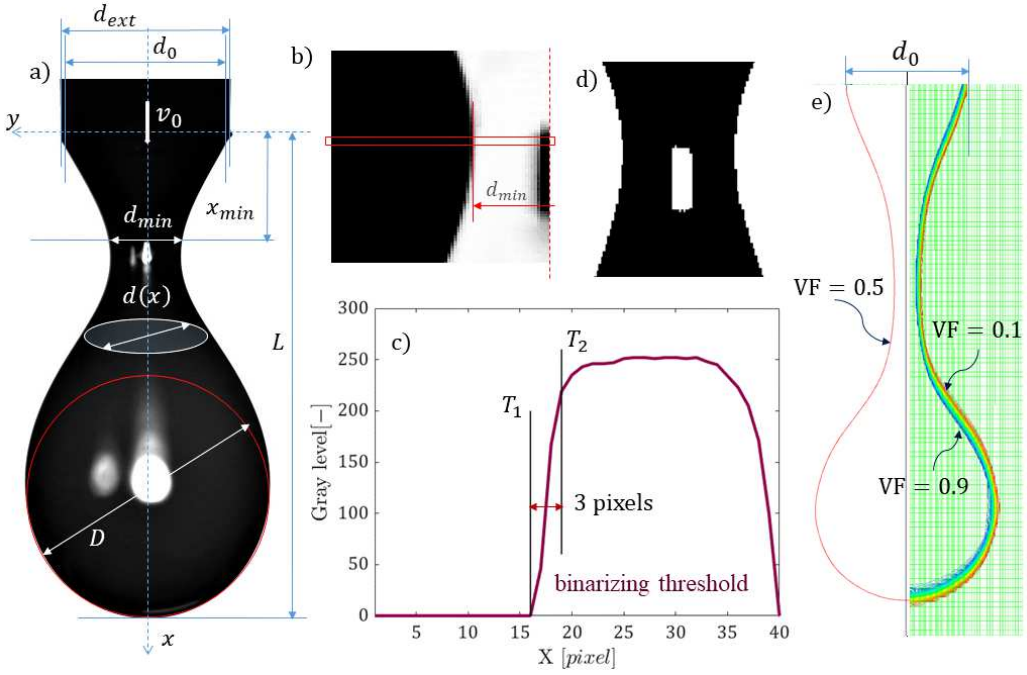

Figure 1. (a) Depiction of the investigated dimensions of a detaching droplet. Steps of the original imagine processing; detail of the neck diameter $d(x) = d_{min}$: (b) negative imagine, (c) distribution of gray levels on the inspection line, corresponding to the minimum thickness of the filament, (d) final binarized image. Numerical interface (e); the mesh/cell size is 27.5 μm and the VF $\in [0.1, 0.9]$ covers 3 cells. The median line VF = 0.5 approximates the computed interface with a maximum error of 42 μm.

The flow dynamics is characterized by the following non-dimensional parameters: Bond – $Bo = \rho g d_0^2/\sigma \cong 1.65$, Reynolds – $Re = \rho v_0 d_0/\eta \cong 0.1$, Weber – $We = \rho v_0^2 d_0/\sigma \cong 0.0076$, capillary – $Ca = \eta v_0/\sigma \cong 0.08$, Ohnesorge – $Oh := \sqrt{Ca/Re} \cong 0.9$, the process being scaled by the viscous and capillary times: $t_v = \eta d_0/\sigma \cong 0{,}017\ s$ and $t_\sigma = \sqrt{\rho d_0^3/\sigma} \cong 0.019\ s$, respectively. Here d_0 and v_0 were considered the space scale and the velocity scale, respectively.

Results and Discussions

The experimental and numerical droplet profiles. In the investigated dynamical process, the capillary force dominates inertia (Ca, We are much less than one) being balanced by the mass force ($0.5 < Bo < 1.5$). Viscosity is equilibrated by the capillarity (Oh almost equal to unity) and inertia is not too relevant for the dynamics ($Re < 1$). Therefore, we have a well-defined dripping regime, in the vicinity of the Stokes flow. Accordingly to the self-similar solution of the Stokes jet flow[2-4], it is expected to find in the very vicinity of the rupture a linear increasing of the minimum diameter of the filament (d_{min} in Fig. 1a) with the relative time: $\tau := t_c - t$, where t_c is the time of the pinch-off (i.e. rupture time of the filament) and t is the current time. However, the scaling dependence of d_{min} with τ depends on the Oh number and the equilibrium between the viscous and capillary forces is perturbed by inertia (especially if the thickness of the filament is not thin)[7,12]. In our experiments the viscous time and the capillary time are almost equal, they are being considered appropriate scales for the process[12]. However, the time value in the range of 17 ms to 20 ms indicates the duration of the linear regime previously the pinch-off (dominated by viscosity and capillarity). The dynamics of the droplet and its profile are displayed in Fig. 2a. for the interval of 100 ms before the observable pinch-off. The evolutions of the droplet contours are shown in Fig. 3a-b, where $\kappa^*(x) = d(x)/d_0$ is the non-dimensional local diameter, Fig. 1a. We have to remark that in numerical simulations the thickness of the needle was not considered, $\kappa^*(0) = 1$ in Fig. 3a. In almost all experiments the fluid wets the needle; therefore, the initial fluid diameter of the experimental data is $d_{ext} = 2.7\ mm$, respectively $\kappa^*(0) = 1.22$ in Fig. 3b. As consequence, in experiments the filament pinch-off is expected to be delayed in comparison with the numerical simulations.

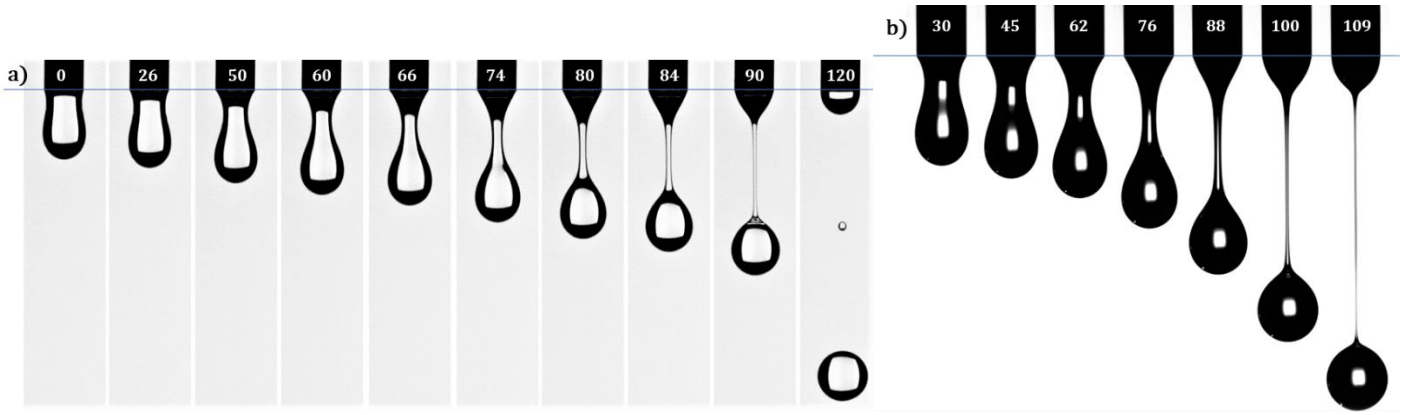

Figure 2 Dynamics of the droplet formation and the evolution of the neck filament of silicon oil in air at $v_0 = 10$ mm/s; (a) experiment E1 – white droplets (2000 fps), (b) experiment E2 – black droplets (4000 fps), The recorded L - length in time is almost identically for the experiments and numerics (see supplementary information).

Time variation of the minimum diameter and thinning velocity. The evolutions of the minimum non-dimensional diameter $\kappa(\tau) = d_{min}/d_0$ are shown in Fig. 4.a-b. The two sets of the experimental data are fitted in Fig. 4b with the S-curve represented by 4PL , the 4th – parameters logistic function $\kappa(\tau) = a_2 + \frac{a_1 - a_2}{1+(\tau/\tau_0)^p}$ or with the S-logistic function $\kappa(\tau) = a\left(1 + b \cdot e^{-k\tau}\right)$, where a_1, a_2, τ_0, p and a, b, k are constants (the values are given in Fig. 4b).

The choosing of 4PL function for fitting the data is suggested by the equilibrium of the normal stresses for a slender jet, where inertia is balanced by the normal extra-stresses difference and the surface tension[4]. Assuming that inertia

force in proportional to the thinning velocity, the surface force is proportional with the area and the capillary force with the diameter, one results the equation: $d\kappa/d\tau = c_1\kappa^2 + c_2\kappa$ with the classical S-logistic function as solution (here c_1 and c_2 are material/process coefficients assumed here to be constants). Of course, this relation is just a qualitative approximation of the local dynamics, but its solution offers a fair fitting of the experiments and of the 4PL function for $\tau > 20\ ms$ (up to the onset of the VR-regime).

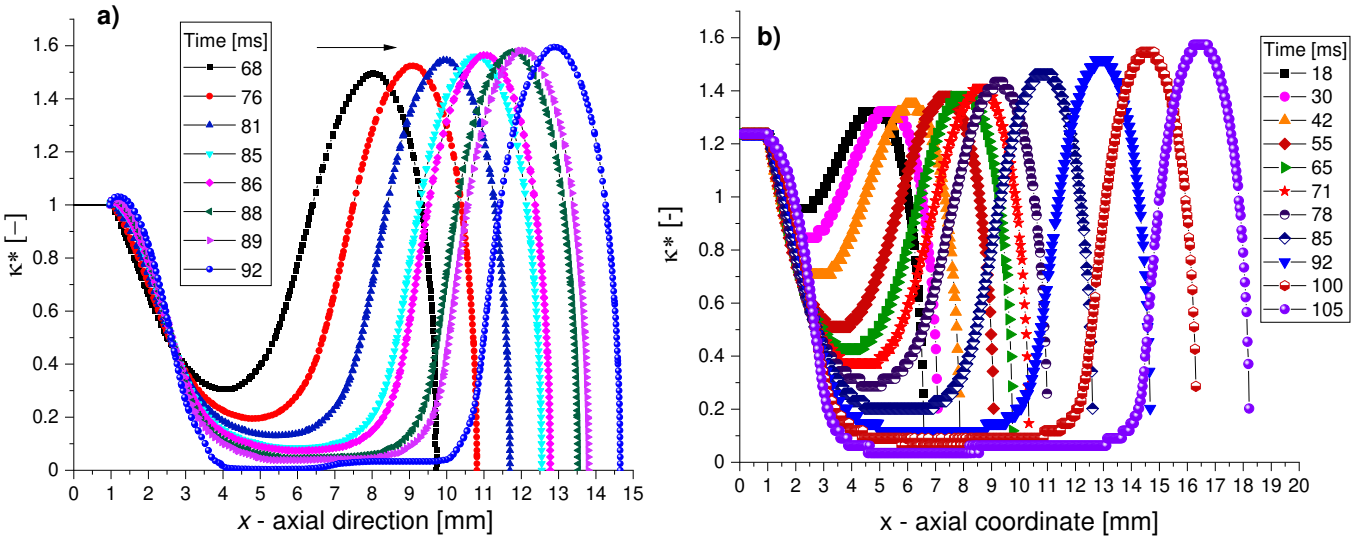

Figure 3. The contours of the droplet at different times, before the detachment from the needle: (a) numerical solutions at VF = 0.5, (b) experiments E2, Fig. 2b.

The relative time variations of L, x_{min} and $dL/d\tau$ (corresponding to the experimental E2 data) are plotted in Fig. 4c. The experimental and numerical thinning velocity $d\kappa/d\tau$ are represented in Fig. 4d. The variations from Figs. 4 disclose the existence of three flow regimes[12]: (i) inertial – capillary (IR) where the filament neck follows at the beginning the scaling $\kappa \sim \tau^{2/3}$, and the thinning velocity is increasing, (ii) transitory (TR) – balance between inertia-capillary and viscous friction, where the thinning velocity reaches the maximum, (iii) viscous – capillary (VR) linear regime characterized by the decreasing of thinning velocity to a constant value ($\kappa \sim \tau$) in the vicinity of the pinch-off. Similar dynamics were observed in different tested configurations, droplet detachment experiments[9-12] or in CaBER rheometer[14-19]. It is remarkable in our results the qualitative correlation between the dynamics of the length L and the minimum diameter κ, in both time dependences $\kappa(\tau)$, Fig. 4a, and $dL/d\tau\ (\tau)$, Fig. 4c, the flow regimes being well defined. We notice that thinning velocity reaches a maximum before the onset of the VR-regime, where the oscillation of x_{min} starts to be amplified. It is generally admitted that in the final stage the thinning velocity is constant[2-4,7,12]. The validity of experimental and numerical results are limited by the space error in the detection of the interface profile and filament thickness (the error in our work is in the range of 30 μm to 40 μm, Fig. 1). Therefore, the present results lack of precision in the very vicinity of the pinch-off at $\kappa < 0.03$ and $\tau < 4\ ms$. Hence, we cannot confirm or infirm that previously to filament rupture the thinning velocity is constant.

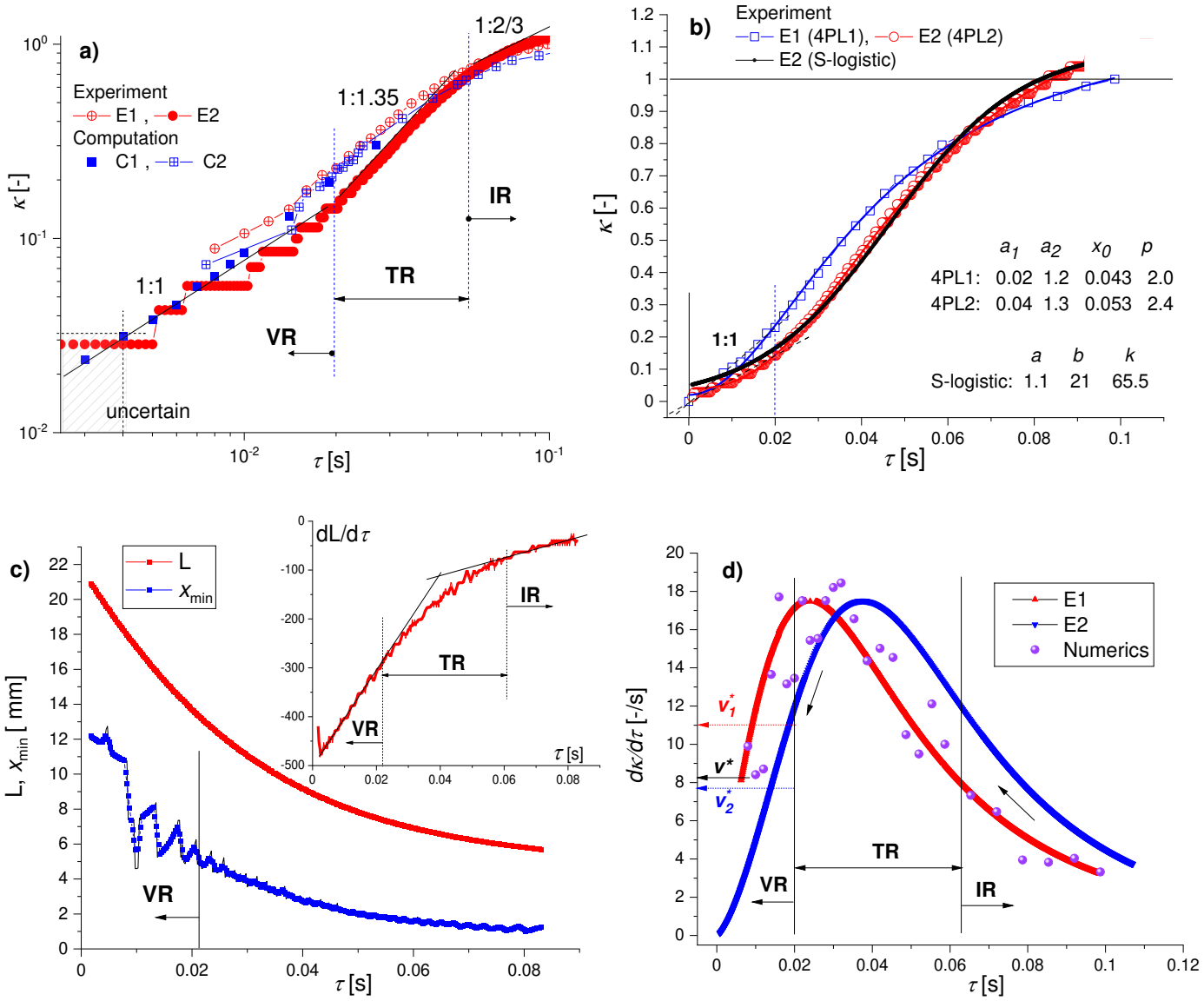

Figure 4. (a) Minimum neck diameter $\kappa = d_{min}/d_0$ as function of the relative time τ (experiment and numerics from Fig. 2), the scaling of κ with τ in the 3 flow regimes: VR – viscous, TR – transitory, IR – inertial; (b) fitting of the experimental curves $\kappa(\tau)$; (c) variation of L and x_{min} (see Fig. 1) for the experimental data E2; (d) the thinning velocity $d\kappa/d\tau$; the value $v^* \cong 8$ [-/s] is given by the formula[3,4] $d\kappa/d\tau = 2 \cdot 0.0709/t_v$. Constant velocities v_1^* and v_2^* corresponds to the linear dependence $\kappa(\tau)$ from (a, b).

Kinematics of the filament's elongation. Droplet formation at low Reynolds numbers, followed by droplet detachment and pinch-off generates (in confined symmetric geometries with symmetric boundary conditions) symmetric vortical structures inside the injected liquid and in the outer fluid[42]. These unsteady vortical structures are connected, deforming with the interface of the droplet, and diffusing in the whole surrounding fluid domain. One measure of vortex existence in a flow field is the magnitude of the local vorticity number $\mathcal{Wo} = |\mathbf{\Omega}|/|\mathbf{D}|$, where $\mathbf{\Omega}$ is the spin tensor and $\mathbf{D}$ is the strain rate tensor (i.e. vorticity number is the ratio between the local vorticity magnitude ω and the local strain rate $\dot{\gamma}$)[43]. The necessary condition (but not a sufficient one !) for the existence of the vortex in a flow domain is $\mathcal{Wo} > 1$. The value $\mathcal{Wo} = 1$ is valid not only at the solid walls or interfaces in contact with pure

viscous fluids (where the adherence condition is valid), but also in simple shear motions (included in the class of flows with solenoidal acceleration). There are some other criteria to characterize and to quantify the local flow kinematics, one being the ζ- coefficient[44], $\zeta = (1 - \mathcal{W}\sigma)/(1 + \mathcal{W}\sigma)$. The ζ- coefficient takes any value in the interval -1 to +1: (i) $\zeta = -1$ defines a pure rotation, (ii) $\zeta = 0$ indicates a simple shear motion and, (iii) $\zeta = +1$ defines a pure extensional flow. In the present study ζ- coefficient is used as a criterion to detect the flow region on the interface where extension is dominant[45]. Fig. 5.

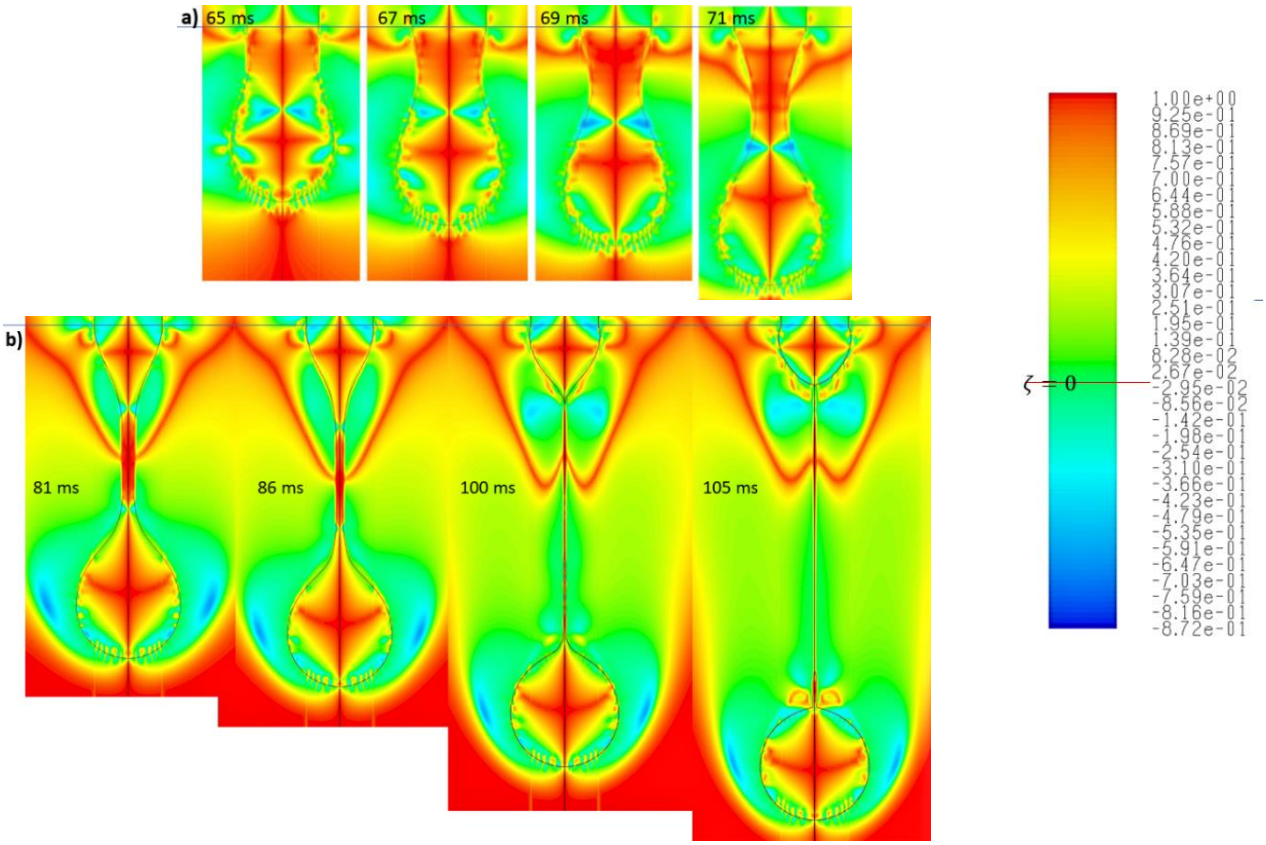

Figure 5 Distribution of ζ – coefficient in the droplet and in its vicinity: TR-regime (a) and VR-regime (b).

The axial velocity distribution $v_{ax}(x)$ on the interface from Fig. 6a indicates the rupture time, i.e. $\tau = 0$, in the vicinity of $t = 100\ ms$ (see Fig. 2). As we observed from Fig. 4, the transition between TR and VR regimes takes place around $t \cong 80\ ms$ ($\tau \cong 20\ ms$). The pattern of ζ- coefficient from Fig. 5 is different in the two regimes. In TR-regime, $t < 80\ ms$ (Fig. 5a), the vortical regions (defined by $\zeta < 0$, blue color) are present in the liquid phase (inside the droplet). Once the dynamics enters in the last stage, $t > 80\ ms$, the vortical regions can be observed in air and in the very vicinity of the filament's limits, Fig. 5b. The ζ – distributions from Fig. 6b disclose that pure elongation ($\zeta \cong 1$) is reached almost in the middle of the filament (expected result, but now confirmed by numerics), the extension dominant region ($0 < \zeta < 1$) being limited by local vorticity concentration ($\zeta < 0$). A detailed analysis of the local kinematics of the interface at time 81 ms (at the onset of the VR-regime) is shown in Fig. 6 and Fig. 7. The filament is limited by the extremes values of the axial velocity v_{ax}, where radial velocity v_{rad} and strain rate are zero (A1 and A2 in Fig. 7a,b). The minimum filament thickness corresponds to the maximum strain rate and to the inflection point

in axial velocity distribution, respectively (point M in Fig. 9a-b); it is located in the region where vorticity is minimum (Fig. 7b) and $\xi -$ coefficient is close to unity (between the points B1 and B2 in Fig. 6.b). The vortical structures are present at the interface in the vicinity of points A1 and A2, where vorticity is maximum (Fig. 7b) and $\xi -$ coefficient reaches minimum (negative values) (Fig. 6b).

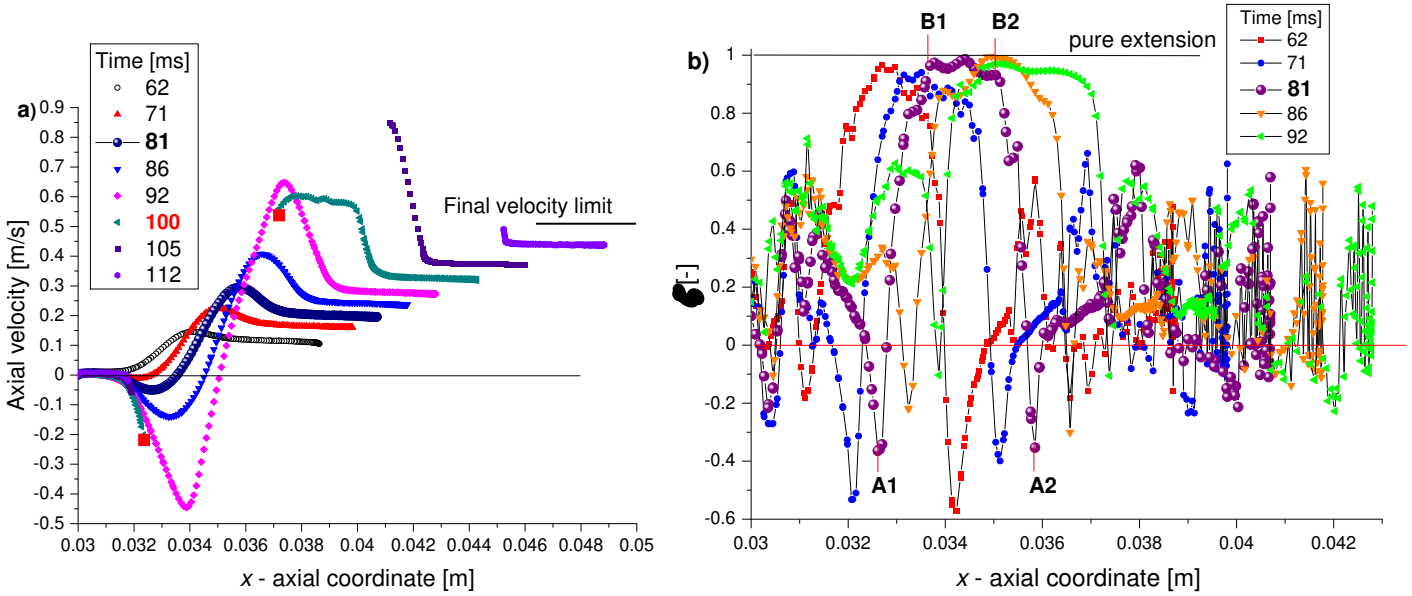

Figure 6. (a) Axial velocity $v_{ax} = v_x$ and (b) $\zeta -$ coefficient distributions on the droplet/filament interface at different values of time (at $t = 81\ ms$ the curves are bolded).

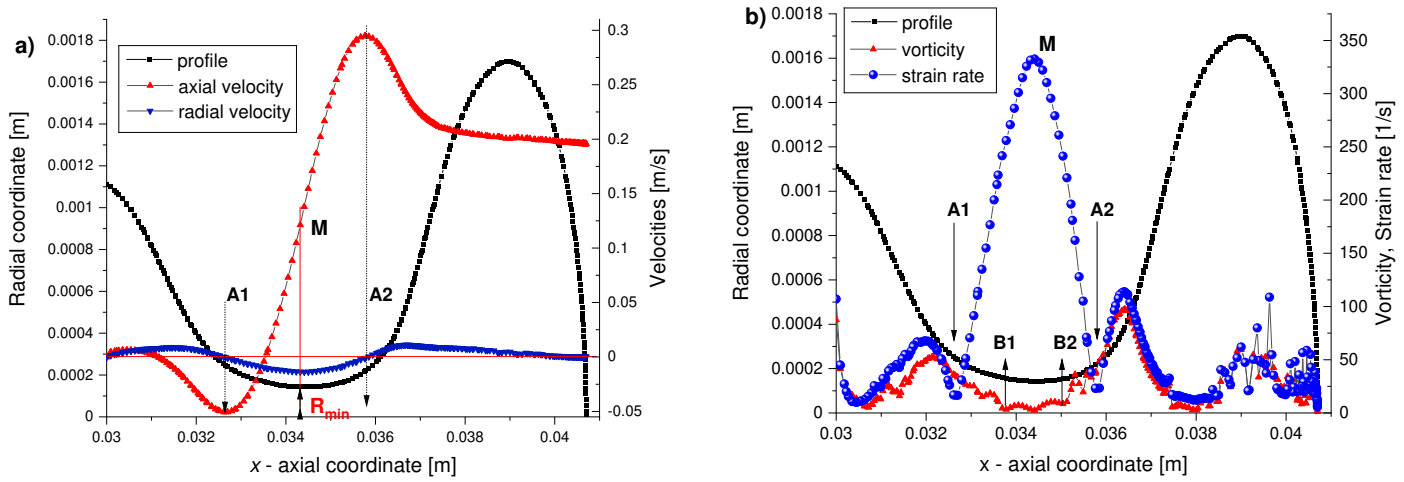

Figure 7. (a) Velocity components, (b) the vorticity and strain rate, along the droplet interface at time $t = 81\ ms$.

The numerical simulations are qualitatively and quantitatively confirmed by the experiments, the results being coherent and consistent with the previous studies dedicated to the filament break-up phenomenon. The analyzed case discloses that thinning velocity of the filament reaches maximum at the onset of the viscous regime and the evolution of the minimum diameter of the filament against the relative time is well fitted by a S-curve (not confirmed in the very vicinity of the filament rupture). Using the computed kinematics, the regions where the motion is close to pure extension on the surfaces of the filaments are precisely located. From the numerical results one can be computed two Reynolds numbers which define the thinning process: (i) $Re_m = \rho v_m d_{min}/\eta$, where v_m is the axial

velocity corresponds to the minimum diameter (at $x = x_{min}$) and (ii) the local Reynolds number – $Re_{local} = \rho v' x'/\eta$, where $x' = x_{1.2 \cdot x_{min}} - x_{min}$ and $v' = v_{ax}(x')$, parameter introduced by Castrejón-Pita, J.R. et al[12]. The two Reynolds numbers have opposite monotonous variations during the filament's thinning previous to the breakup. In the transitory and viscous regimes Re_m is decreasing and Re_{local} is increasing, with the following values in the vicinity of pinch-off (at $\tau = 0.006\ s$ and $\kappa \cong 0.04$, Fig. 4a): $Re_m = 0.0095$ and $Re_{local} = 6.52$, respectively. It is important to mention that onset of viscous regime is well defined by a sharp change of the time derivative for both Reynolds numbers. In the viscous regime, at $\tau < 0.02\ s$, $Re_m < 0.1$ and $Re_{local} > 1$. The values of Re_m indicates the presence of the Stokes flow before rupture, which support the existence of a constant thinning velocity in that regime.

Concluding remarks

The present work investigated the formation and breakup of viscous droplet in air. The main goal of the study is to characterize the flow kinematics on the surface of the filament, with the aim to establish the region with maximum extension. The main parameter followed in our investigations was the evolution of the filament neck in the vicinity of the droplet pinch-off. The numerics offer a good representation of the phenomenon. The computations are consistent with experiments, except for the region in the very vicinity of thread rupture, where the errors in the measurements and computations have the magnitude of the filament thickness.

Some relevant remarks follow the analysis of the thinning of the minimum filament diameter (i.e. the dependence of the non-dimensional diameter κ against the relative time τ): (i) a monotonous increasing of the neck thinning velocity where inertia and capillarity are balanced, followed by (ii) a transition regime characterized by the equilibrium between inertia, capillarity and viscous force, where thinning velocity varies non-monotonic and (iii) the final pinch-off regimes, where velocity is decreasing or oscillates around a constant value. The decreasing of $\kappa(\tau)$ function is well approximated by logistic functions, the S-curves fit almost perfect the data up to the vicinity of the filament's rupture (however, in this region the uncertainty of the filament profile is high; additional experiments for different liquid samples can be found in the supplementary information).

Once the numerical calculations are validated by the experiments, relevant information can be obtained about the kinematics of the investigated flows on the interface: (a) the distributions of velocities and strain rates, (b) the location of the vortical structures and vorticity magnitude, (c) the regions where pure extension is present. In this paper we emphasize the importance of the ζ- coefficient distribution on the droplet/filament profile. The process of breaking is dominated by elongational deformation; in the vicinity of the pinch-off $\zeta > 0$ on the filament surface and inside the droplet. The analysis of ζ- coefficient distribution on the interface reveals the regions where the process is almost pure extensional ($\zeta \cong 1$), which coincide with a domain around the minimum thickness of the filament.

Finally, one concludes that ζ- coefficient distribution on the separation surface between immiscible fluids can be considered a relevant parameter to analyze the kinematics of interfaces; in particular, to detect the places on the interface characterized by pure extension. The results have potential in developing novel techniques and more precise procedures in measuring the interfacial rheological properties of viscous and complex fluids in dominated elongational flows.

References

1. Eggers, J. Universal pinching of 3D axisymmetric free surface flow, *Phys. Rev. Lett.* **71**, 3458-3460(1993)
2. Eggers, J. & Dupont, T.F. Drop formation in a one-dimensional approximation of the Navier–Stokes equation, *J. Fluid Mech.* **262**, 205–221 (1994).
3. Papageorgiou, D.T. On the breakup of viscous liquid threads, *Phys. Fluids* **7**, 1529-1544 (1995).
4. Papageorgiou, D.Y. Analytical description of the breakup of liquid jets, *J. Fluid Mech.* **301**, 109-132 (1995).
5. Zhang, X. & Basaran, O.A. An experimental study of dynamics of drop formation, *Phys. Fluids* **7**, 1184-1203 (1995).
6. Eggers, J. Nonlinear dynamics and breakup of free-surface flows, *Rev. Modern Phys*. **69**, 865–929 (1997)
7. Day, R.F., Hinch, E.J. & Lister, J.R. Self-similar capillary pinchoff of an inviscid fluid. *Phys. Rev. Lett*. **80**, 704-707 (1998).
8. Clanet, Ch. & Lasheras, J.C. Transition from dripping to jetting, *J. Fluid Mech*. **383**, 307-326 (1999).
9. Ambravaneswaran, B., Wilkes, E.D. & Basaran, O.A. Drop formation from a capillary tube: comparison of one dimensional and two-dimensional analyses and occurrence of satellite drops, *Phys. Fluids* **14**, 2606-2621 (2002).
10. Rothert, A., Richter, R. & Rehberg, I. Formation of a drop: viscosity dependence of three flow regimes, *New J. Phys*. **5**, 59.1-59.13 (2003).
11. Notz, P.K. & Basaran, O.A. Dynamics and breakup of a contracting liquid filament, J. Fluid Mech. **512**, 223–256 (2004).
12. Castrejón-Pita, J.R. et al. Plethora of transitions during breakup of liquid filaments, *Proc. Natl. Acad. Sci. USA* **112**, 4582–4587 (2015).
13. Szabo, P. Transient filament stretching rheometer, Rheol. Acta **36**, 277-284 (1997).
14. McKinley, G.H. & Sridhar, T. Filament-stretching rheometry of complex fluids, *Annu. Rev. Fluid Mech*. **34**, 375–415 (2002).
15. Anna, S.L. & McKinley, G.H. Elasto-capillary thinning and breakup of model elastic liquids, *J. Rheol*. **45**, 115-137 (2001).
16. Tirtaatmadja, V., McKinley, G.H. & Cooper-White, J.J. Drop formation and breakup of low viscosity elastic fluids: Effects of molecular weight and concentration, *Phys. Fluids* **18**, 043101 (2013).
17. Yildirim, O.E. & Basaran, O.A. Deformation and breakup of stretching bridges of Newtonian and shear-thinning liquids: comparison of one-and two dimensional models, *Chem. Eng. Sci.* **56**, 211–233 (2001).
18. Rodd, L.E., Scott, T.P., Cooper-White, J.J. & McKinley, G.H. Capillary break-up rheometry of low-viscosity elastic fluids, *Appl. Rheol*. **15**, 12-27 (2005).
19. Sujatha, K.S., Matallah, H., Banaai, M.J. & Webster, M.F. Modeling step-strain filament-stretching (CaBER-type) using ALE techniques, *J. Non-Newt. Fluid Mech.* **148**, 109-121 (2008).
20. Tuladhar, T.R. & Mackley, M.R. Filament stretching rheometry and break-up behavior of low viscosity polymer solutions and inkjet fluids, *J. Non-Newt. Fluid Mech*. **148**, 97-108 (2008).
21. Aytouna, M. et al. Drop formation in non-Newtonian fluids, Phys. Rev. Lett. **110**, 034501 (2013).
22. Zhang, D.F. & Stone, H.A. Drop formation in viscous flows at a vertical capillary tube, *Phys. Fluids* **9**, 2234-2242 (1997).
23. Dravid, V., Loke, P.B., Corvalan, C.M. & Sojka, P.E. Drop formation in non-Newtonian jets at low Reynolds numbers, *J. Fluids Eng*. **130**, 081504 (2008).
24. Patrascu, C. & Balan, C. Temporal instability of a viscoelastic liquid thread in the presence of a surrounding viscoelastic fluid, *J. Non-Newt. Fluid Mech.* **261** (2018) 164-170.
25. Deblais, A., Herrada, M.A., Eggers, J. & Bonn, D. Self-similarity in the breakup of very dilute viscoelastic solutions, *J. Fluid Mech*. **904**, R2 (2020).

26. Pingulkar, H., Peixinho, J. & Crumeyrolle, O. Drop dynamics of viscoelastic filaments, *Phys. Rev. Fluids* **5**, 10.1103 (2020).
27. McKinley, G.H. & Tripathi, A. How to extract the Newtonian viscosity from capillary breakup measurements in a filament rheometer, *J. Rheol.* **44**, 653-670 (2000).
28. Sur, S. & Rothstein, J. Drop breakup dynamics of dilute polymer solutions: Effect of molecular weight, concentration, and viscosity, *J. Rheol.* **62**, 1245-1259 (2018).
29. Basaran, O.A., Gao, H. & Bhat, P.P. Nonstandard Inkjets. *Annu. Rev. Fluid Mech.* **45**, 85-113 (2013).
30. Mathues, W., McIlroy, C., Harlen, O.G. & Clasen, C. Capillary breakup of suspensions near pinch-off, *Phys. Fluids* **27**, 093301 (2015).
31. Turcanu, M., Siegert, N., Secouard, S., Brito-de la Fuente, E., Balan, C. & Gallegos, C. An alternative elongational method to study the effect of saliva on thickened fluids for dysphagia nutritional support, *J. Food Eng.* **228**, 79-83 (2018).
32. Hadde, E.K., Cichero J.A.Y., Zhao S., Chen W. & Chen J. The importance of extensional rheology in bolus control during swallowing, *Scie. Report Nat.* **9**, 16106; 10.1038/s41598-019-52269-4 (2019).
33. Marshall, K.A. & Walker, T.W. Investigating the dynamics of droplet breakup in a microfluidic cross-slot device for characterizing the extensional properties of weakly-viscoelastic fluids, *Rheol Acta* **58**, 573-590 (2019).
34. Valette, R., Hachem, E., Khalloufia, M., Pereira, A.S., Mackley, M.R. & Butler, S.A. The effect of viscosity, yield stress, and surface tension on the deformation and breakup profiles of fluid filaments stretched at very high velocities, *J. Non-Newt. Fluid Mech.* **263**, 130-139 (2019).
35. Metaxas, A.E., Coughlin, M.L., Hansen, C.K, Bates, F.S., Lodge, T.P. & Dutcher, C.S. Microfluidic filament thinning of aqueous, fibrillar methylcellulose solutions, *Phys. Rev. Fluids* **5**, 113302, (2020).
36. P. Zhu, X. Tang, Y. Tian & L. Wang, Pinch-off of microfluidic droplets with oscillatory velocity of inner phase flow, *Scie. Reports Nat.* **6**, 31436; 10.1038/srep31436 (2016).
37. Martínez-Calvo, A. & Sevilla, A. Universal thinning of liquid filaments under dominant surface forces, *Phys. Rev. Letters* **125**, 114502 (2020).
38. Hirt, C.W. & Nichols, B.D. Volume of Fluid (VOF) method for the dynamics of free boundary, *J. Comput. Phys.* **39**, 201–225 (1981).
39. Wilkes, E.D., Phillips, S.D. & Basaran, O.A. Computational and experimental analysis of dynamics of drop formation, *Phys. Fluids* **11**, 3577-3598 (1999).
40. Lörstad, D., Francois, M., Shyy, W. & Fuchs, L. Assessment of volume of fluid and immersed boundary methods for droplet computations, *Int. J. Numer. Meth. Fluids* **46**, 109–125 (2004).
41. Fawehinmi, O.B., Gaskell, P.H., Jimack, P.K., Kapur, N. & Thompson, H.M. A combined experimental and computational fluid dynamics analysis of the dynamics of drop formation, *J. Mech. Eng. Scie.* **219**, 1989-1996 (2005).
42. Jeong, J. & Hussain, F. On the identification of a vortex, *J. Fluid Mech.* **285**, 69-94 (1995).
43. Truesdell, C. Two measures of vorticity, *J. Ratio. Mech. Anal.* **2**, 173-217 (1953).
44. Astarita, G. Objective and generally applicative criteria for flow classification, *J. Non-Newtonian Fluid Mech.* **6**, 69-76 (1979).
45. Haward, S.J., McKinley G.H. & Shen A.O., Elastic instabilities in planar elongational flow of monodisperse polymer solutions, *Scie. Reports Nat.* **6**, 33029; 10.1038/srep33029 (2016).

Acknowledgements

The experiments were possible due to the European Regional Development Fund through Competitiveness Operational Program 2014-2020, Priority axis 1, Project No. P_36_611, MySMIS code 107066, Innovative Technologies for Materials Quality Assurance in Health, Energy and Environmental - Center for Innovative Manufacturing Solutions of Smart Biomaterials and Biomedical Surfaces – INOVABIOMED.
The authors acknowledge the financial support of CHIST-ERA – 19 – XAI – 009 MUCCA project, by the founding of EC and The Romania Executive Agency for Higher Education, Research, Development and Innovation Funding - UEFISCDI, grant COFUND-CHIST-ERA MUCCA no. 206/2019.

Author contributions

D.B. performed the numerical simulations, A-M. B. And I. M. performed the experiments and analysed the data, C.P. designed the experiments and proofread the manuscript, C.B. coordinated the work and wrote the main manuscript text. All authors approved the submitted version.

Competing interests

The authors declare no competing interests.

Additional information

Supplementary information accompanies this paper ...
Correspondence and requests for materials should be addressed to C.B.

Supplementary Files

This is a list of supplementary files associated with this preprint. Click to download.

- PaperC.BalanSupplementaryInformation.pdf